Journal of Stress Analysis
Vol. 1, No. 2, Autumn – Winter 2016-17
Bu-Ali Sina University

An Approach to Designing a Dual Frequency Piezoelectric Ultrasonic Transducer

A. Pak[a,*], A. Abdullah[b]

[a]Mechanical Engineering Department, Faculty of Engineering, Bu-Ali Sina University, Hamadan, Iran.

[b]Mechanical Engineering Department, Faculty of Engineering, Amirkabir University of Technology, Tehran, Iran.

Article info

Article history:
Received 2017.01.04
Received in revised form 2017.02.06
Accepted 2017.03.01

Keywords:
Dual frequency ultrasonic transducer
High power ultrasonic
FEM simulation
Ultrasonic cleaning

Abstract

This paper has been devoted to such approach for designed and fabricated the dual frequency piezoelectric ultrasonic transducer having longitudinal vibrations for high power application. By using analytical analysis, the resonance frequency equations of the transducer in the half-wave and the all-wave vibrational modes were determined for the assumed first resonance frequency of 25kHz. According to the resonance frequency equation, four transducers with two different constructions (Type A and B) were designed and made. The finite element method provided by commercial ANSYS was employed for FEM modeling and analysis of the transducer to observe its vibration behavior. It was shown that there is a good agreement between the experimental and FEM results. The designed and fabricated transducer can be excited to vibrate at two resonance frequencies, which correspond to the half-wave and the all-wave vibrational modes of the transducer, and use of Type B transducer greatly increased the mechanical quality factor (Q) of piezoelectric transducers.

Nomenclature

$A\ (m^2)$	Cross-section	$\rho\ (Kg/m^3)$	Density
ν	Poisson's ratio	$\omega\ (Hz)$	Angular resonant frequency
$C\ (m/s)$	Sound speed	$C_m\ (F)$	Equivalent compliance
$C_s\ (F)$	Static capacitance of piezoelectric	$d\ (C/N)$	Piezoelectric charge constant
$f\ Hz$	Resonant frequency of transducer	$L\ (m)$	Length
$L_m\ H$	Equivalent motional mass	Q	Quality factor
R_m	Dissipative power loss	$t\ (sec)$	Time
$T\ (N/m^2)$	Stress	$u\ (m)$	Displacement
$Y\ (N/mm^2)$	Youngs modulus	ε_r^s	Dielectric relative permittivity
$\lambda\ (m)$	Wave length		

1. Introduction

Application of high intensity ultrasonic waves has been considerably progressed during the last decade and conventional Langevin or sandwich transducers have had a common use as the driving source of such waves. Traditional ultrasonic-transducers' sandwich structure is operated only on one resonance frequency. There have been great efforts to optimize and improve such transducers and their applications [1-5]. However, to produce ultrasound with different frequencies, a multi-frequency ultrasonic transducer should be used. This presents a new subject for ultrasonic cleaning and ultrasonic liquid processes. In the case of dual frequency ultrasonic cleaning, there exist waves with different frequencies in the cleaning tank, the standing wave is

*Corresponding author: A. Pak (Assistant Professor)
E-mail address: a.pak@basu.ac.ir

destroyed and the difference between the nodes and antinodes is decreased. Therefore the cleaning quality can be improved. In recent decades, there has been some interest in designing dual frequency piezoelectric transducer by means of two groups of piezoelectric ceramic elements. One group is used as the active element which is connected to an electrical generator; the other group is used as the controlling elements which are connected to inductance or capacitance. When the inductance or capacitance is changed, the resonance frequency can be adjusted by means of the piezoelectric effect [6-8]. Lin and Xu [9] presented the analysis of a sandwich transducer with two sets of piezoelectric ceramic elements which are separated by a middle metal cone. The two sets of piezoelectric elements are excited separately, and therefore two groups of resonance and anti-resonance frequency can be obtained. Lin [10] also studied an improved cymbal transducer that consists of a combined piezoelectric ring and metal ring, and metal caps. In another paper, Lin et al. [11] studied a composite transducer that consists of a sandwich longitudinal piezoelectric transducer, an isotropic metal hollow cylinder with large radial dimension, and the front and back metal radiation mass. In their paper, the resonance frequency was found analytically by electrical equivalent circuit model method. Finally, they manufactured some transducers and measured the resonance frequency and the radiation acoustic field in order to compare them with the analytical and numerical results. Deniz [12] studied numerical and experimental design of a multi-frequency underwater acoustic transducer with two sets of piezoelectric tubes. In this study, one of the tubes operated at about 30kHz and the other one at about 60kHz. Asami and Miura [13] investigated a new type of ultrasound longitudinal-torsional vibration source consisting of a longitudinal transducer and a torsional transducer at opposite ends of a uniform rod as a vibration source. The individual vibrations could be controlled. The longitudinal vibration distributions for driving only the longitudinal transducer and the torsional vibration distributions for driving only the torsional transducer were similar in the uniform rod.

In this paper a modification on the sandwich structure was implemented by employing two different constructions; Type A, in which the center mass was not connected to the central bolt and the central bolt could be approximately considered as the rigid connection between two end metal masses and Type B, in which the central bolt mechanically connected all masses (Fig. 1). The aim of this research is to investigate the behavior of the proposed ultrasonic transducers in order to discover the modes of vibration and proper construction and the material of the central mass. These transducers were analyzed by theoretical, numerical and experimental methods. The analyzed transducers were composed of four piezo-ceramic rings, PZT-SA, a steel cylinder-shaped back mass (St 304), an Aluminum cylinder-shaped front mass (Al 7075-T6) and a steel cylinder-shaped central mass (SA and SB) and an Aluminum cylinder-shaped central mass (AA and AB). The configurations of modeled and designed ultrasonic transducers are shown in Fig. 2.

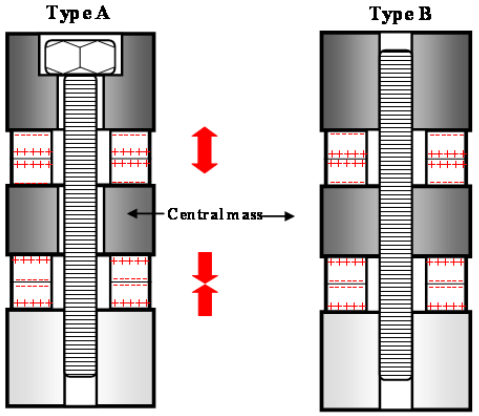

Fig. 1. Ultrasonic transducers: Type A (Center mass connected directly to bolt) and Type B (Center mass moves independently of the bolt).

By using the analytical method and assuming a certain resonant frequency and a power, the resonance frequency equations of the transducer and the dimensions of the components were determined. Then, the finite element analysis provided by ANSYS was employed for FEM analysis to observe the vibration behavior of the transducer and to verify the validity of the analytical calculations. Finally, the analytical analysis results, simulation results of FEM, and experimental results were compared and discussed.

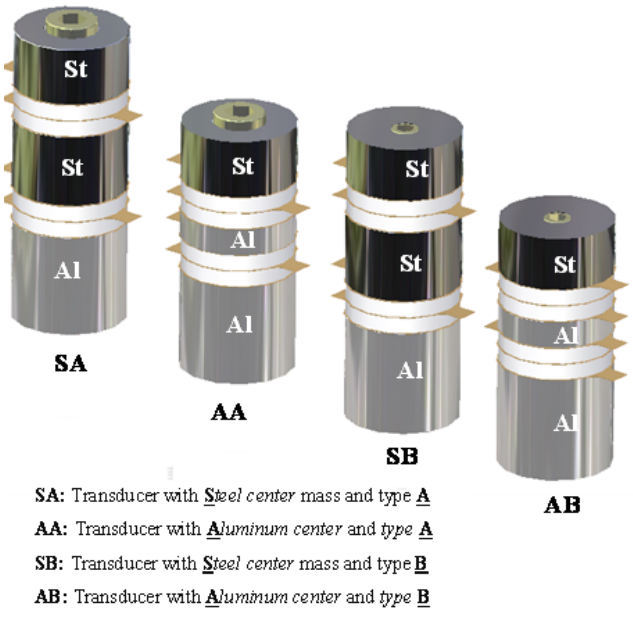

Fig. 2. The Configuration of modeled and designed ultrasonic transducers.

2. Theoretical Analysis of the Dual Frequency Piezoelectric Transducer

Fig. 3 shows the transducer with a center mass. In this figure, L_b, $2L_c$, and L_f are the lengths of the back mass, the central cylinder mass and the front metal mass respectively; each having a circular cross-section. Two groups of piezoelectric ceramic driving elements whose lengths are L_p, are separated by the center mass. To simplify the theoretical analysis, the following assumptions were made:
Lateral pressure on the transducer is zero and sinusoidal longitudinal plane waves propagate axially. Diameter variation along transducer is also far enough from the critical value. Mean while, the influence of fillets and chamfers in the corners are ignored. Therefore, lateral or radial modes of vibration are negligible and the problem is one-dimensional.

Maximum diameter of the transducer is less than a quarter of the sound wavelength and the relationship $c = \sqrt{\frac{Y}{\rho}}$ can be used with relatively accurate approximation (where c is the sound speed in media with elasticity module of Y and density of ρ) [14]. The total length of the transducer is appropriate to standing waves generation. Acoustic impedance of air is considered zero so that a transducer operating in air is said to be unloaded.

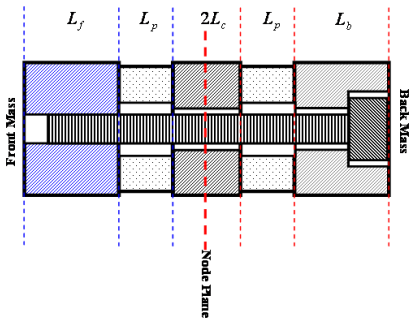

Fig. 3. The geometrical diagram of the ultrasonic transducers with two frequencies (Type A).

The most fundamental rule in determination of various axial dimensions in the transducer is to permit it to operate in resonance, the overall length should be exactly $\frac{\lambda}{2}$ (or a whole coefficient of $\frac{\lambda}{2}$). Since the transducer is not a single body and consists of several parts with different materials and cross-sections along the transducer, the following analytical relationship for one-dimensional longitudinal sinusoidal plane wave propagation in medium is applied [15]:

$$\frac{d^2u_i}{dx_i^2} + \frac{1}{A_i}\frac{dA_i}{dx_i}\cdot\frac{du_i}{dx_i} + \frac{w_n^2}{C_{0_i}^2}u_i = 0 \qquad (1)$$

Equation (1) is simplified to the following differential equation for each section through which the cross-section is constant $\left(\frac{dA_i}{dx_i} = 0\right)$:

$$\frac{d^2u_i}{dx_i^2} + k_i^2 u_i = 0 \qquad (2)$$

$$k_i = \frac{w}{C_{0_i}} \qquad (3)$$

Depending on the boundary conditions and vibrational mode, the resonance frequency equations of the transducer with two frequencies in half-wave and one-wave vibrational mode can be obtained.

2.1. The Resonance Frequency Equations of the Transducer in the Half-wave Vibrational Mode

In this case, the transducer can be regarded as a longitudinal vibrator of half a wavelength, its two ends are the antinodes, and there is a node in the transducer. Let the node be located in the middle cylinder of the transducer, and divide the center mass into two same cylinders of L_{c1} and L_{c2} ($L_{c1} = L_{c2} = L_c$).

The part after the node plane consists of the center mass of length L_c, the piezoelectric ceramic and the back mass (Fig. 4).

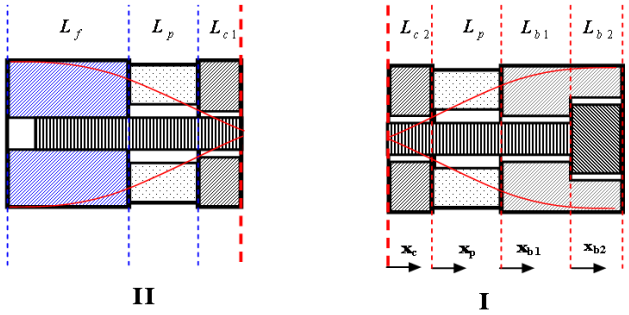

Fig. 4. The geometrical diagram of the transducer in the half-wave vibrational mode (Type A).

Solving the Equation (2) for each section of L_c and L_p and applying the boundary conditions as $u_c(x_c = 0) = 0$, it results:

$$u_c = A_1\sin(k_c x_c) + A_2\cos(k_c x_c)$$
$$A_2 = 0$$
$$u_c = A_1\sin(k_c x_c) \qquad (4)$$

According to Hookes Law and Equation (4) the stress, T, is given by equation:

$$T_c = Y_c = \frac{du_c}{dx_c} = A_1 Y_c k_c\cos(k_c x_c) \qquad (5)$$

where Y (N/m^2) is the Youngs modulus.

$$u_p = A_3\sin(k_p x_p) + A_4\cos(k_p x_p)$$

$$u_p = D_1\sin(k_p x_p + \alpha)$$

where $D_1 = \sqrt{A_3^2 + A_4^2}$ and $\alpha = \tan^{-1}\dfrac{A_4}{A_3}$

$$T_p = Y_p \frac{du_p}{dx_p} = D_1 Y_p k_p \cos(k_p x_p + \alpha) \tag{6}$$

The boundary conditions between the parts are: equilibrium of displacement (continuity condition) and force (Newtons third law) of the two contacting media at the shared plane.

$$u_c = (x = L_c) = u_p(x_p = 0) \implies A_1 \sin(k_c L_c) = D_1 \sin(\alpha) \tag{7}$$

$$F_c = (x_c = L_c) = F_p(x_p = 0), \quad F = T \cdot A \implies A_1 Y_c K_c A_c \cos(k_c L_c) = D_1 Y_p k_p A_p \cos(\alpha) \tag{8}$$

By dividing equation (4) over equation (5) value for α will be:

$$\alpha = \tan^{-1}\left[\frac{Y_p k_p A_p}{Y_c k_c A_c}\tan(k_c L_c)\right]$$

According to the similar procedure by solving Equation (2) for each section of L_{b1} and L_{b2} and applying boundary conditions:

$$u_{b_1} = A_5 \sin(k_b x_{b_1}) + A_6 \cos(b_b x_{b1})$$

$$u_{b_1} = D_2 \sin(k_b x_{b1} + \beta)$$

$$u_{b2} = A_7 \sin(k_b x_{b2}) + A_8 \cos(k_b x_{b2})$$

$$u_{b2} = D_3 \sin(k_b x_{b2} + \varphi)$$

$$u_p(x_p = L_p) = u_{b1}(x_{b1} = 0) \implies D_2 \sin(k_p L_p + \alpha) = D_2 \sin(\beta)$$

$$u_{b1}(x_{b1} = L_{b1}) = u_{b2}(x_{b2} = 0) \implies D_2 \sin(k_b L_{b1} + \beta) = D_3 \cos(k_b L_{b2})$$

$$F_p(x_p = L_p) = F_{b1}(x_{b1} = 0), \quad F = T \cdot A \implies D_1 Y_p A_p \cos(K_p L_p + \alpha) = D_1 Y_b k_b A_{b1} \cos(\beta) \tag{9}$$

$$F_{b1}(x_{b1} = L_{b1}) = F_{b2}(x_{b2} = 0) \implies D_2 Y_b k_b A_{b1} \cos(K_b L_{b1} + \beta) = D_3 Y_b k_b A_{b2} \sin(k_b L_{b2}) \tag{10}$$

$$\beta = \tan^{-1}\left[\frac{Y_b k_b A_{b1}}{Y_p k_p A_p}\tan(k_p L_p + \alpha)\right] = \tan^{-1}\left[\frac{Y_b k_b A_{b1}}{Y_p k_p A_p}\tan\left(k_p L_p + \tan^{-1}\left[\frac{Y_p k_p A_p}{Y_c k_c A_c}\tan(k_c L_c)\right]\right)\right]$$

By dividing Equation (9) over Equation (10) the resonance frequency equation of the part after the node plane (section I) was determined:

$$A_{b_1}\cos\left(k_b L_{b1} + \tan^{-1}\left[\frac{Y_b k_b A_{b1}}{Y_p k_p A_p}\tan\left(k_p L_p + \tan^{-1}\left[\frac{Y_p k_p A_p}{E_c k_c A_c}\tan(k_c L_c)\right]\right)\right]\right)\cos(k_b L_{b2})$$
$$- A_{b_2}\sin(k_b L_{b2})\sin\left(k_b L_{b1} + \tan^{-1}\left[\frac{Y_b k_b A_{b1}}{Y_p k_p A_p}\tan\left(k_p L_p + \tan^{-1}\left[\frac{Y_p k_p A_p}{E_c k_c A_c}\tan(k_c L_c)\right]\right)\right]\right) = 0 \tag{11}$$

The resonance frequency equation of the part before the node plane can be derived according to the similar procedure: The part before the node plane can be regarded as a longitudinal transducer of a quarter wavelength and it consists of the center mass of length L_{c1}, the piezoelectric ceramic, and the front mass.

$$Y_f A_f k_f \sin(k_f L_f) \times \sin\left(k_p L_p + \tan^{-1}\left[\frac{Y_p k_p A_p}{Y_c k_c A_c}\tan(k_c L_c)\right]\right) -$$

$$Y_p A_p k_p \sin(k_p L_p) \times \sin\left(k_p L_p + \tan^{-1}\left[\frac{Y_p k_p A_p}{Y_c k_c A_c}\tan(k_c L_c)\right]\right) = 0 \tag{12}$$

Equations (11) and (12) are the resonance frequency equations of the transducer in half-wave vibrational mode. When the material parameters and the resonance frequency are designated, the transducer can be designed and the dimensions can be calculated from the equations.

2.2. The Resonance Frequency Equations of the Transducer in the Half-wave Vibrational Mode

In this case, apart from the two antinodes at the ends of the transducer there is also an antinode in the transducer. The transducer can be regarded as a combination of two transducers of half a wavelength. As shown in Fig. 5 when the antinode is located at the center mass, it divides the center mass into two cylinders of L_{c1} and L_{c2}, Therefore 2_{Lc} will be:

$$2L_c = L_{c1} + L_{c2} \tag{13}$$

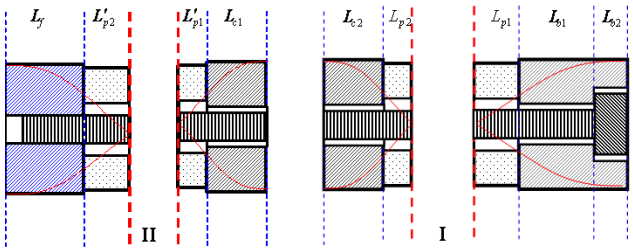

Fig. 5. The geometrical diagram of the transducer in the one wave vibrational mode (Type A).

The half wavelength transducer before the antinode in the center mass consists of the center mass of length L_{c1}, the piezoelectric ceramic (L'_{p1}, L'_{p2}) and the front mass (L_f). When the transducer is unloaded, the stress at the displacement antinode in the center mass is equal to zero, therefore, the half wavelength transducer vibrates freely. Applying the boundary conditions and solving the Equation (2) for each section of part I, the resonance frequency equation of the part before the antinode in the center mass was determined:

$$Y_c A_c \times \frac{w}{c_c} \times \tan\left[\frac{w}{c_c}(L_c - L_{c1})\right] \times \frac{\tan\left(\frac{w}{c_p}L_p\right) - \dfrac{Y_p \times \frac{w}{c_p} \times A_p}{Y_f A_f \frac{w}{c_f} \tan\left(\frac{w}{c_f}L_f\right)}}{1 + \tan\left(\frac{w}{c_p}L_p\right) \times \dfrac{Y_p \times \frac{w}{c_p} \times A_p}{Y_f A_f \frac{w}{c_f} \tan\left(\frac{w}{c_f}L_f\right)}} - Y_p \times \frac{w}{c_p} \times A_p = 0 \qquad (14)$$

The half wavelength transducer after the antinode in the center mass consists of the center mass of length L_{c2}, the piezoelectric ceramic ($L_{p1},\ L_{p2}$) and the back mass ($L_{b1},\ L_{b2}$). The resonance frequency equation of the part II can be derived according to the similar procedure:

$$A_{b1} - A_{b2}\tan\left(\frac{w}{c_b}L_{b2}\right)\tan\left(\frac{w}{c_b} \times L_{b1} + \tan^{-1}\left[\frac{Y_b \times \frac{w}{c_b} \times A_{b1}}{Y_b \times \frac{w}{c_p} \times A_p} \times \frac{\tan\left(\frac{w}{c_p}L_p\right) - \dfrac{Y_p \times \frac{w}{c_p} \times A_P}{Y_c A_c \times \frac{w}{c_c} \times \tan\left(\frac{w}{c_c}L_{c1}\right)}}{1 + \tan\left(\frac{w}{c_p}L_p\right) \times \dfrac{Y_P \frac{w}{c_p} A_p}{Y_c A_c \times \frac{w}{c_c} \times \tan\left(\frac{w}{c_c}L_{c1}\right)}}\right]\right) = 0 \qquad (15)$$

According to the above analysis, the procedures for designing an ultrasonic transducer with two frequencies are as follows. a) When the resonance frequency of the transducer in the half-wave vibrational mode, the material parameters of the components of the transducer, the dimensions of the piezoelectric ceramic and the length of the center mass are given, the length of the back mass and the front mass can be determined from the resonance frequency equations (Equations (11) and (12)) b) The next procedure is to determine the resonance frequency of the transducer in the all-wave vibrational mode.

In the resonance frequency equations (Equations (14) and (15)), there are two unknowns. They are Lc1 and the resonance frequency of the transducer in the all-wave vibrational mode ($w = 2\pi f$). As Equations (14) and (15) are transcendental ones, the analytic solutions are difficult to obtain; therefore, numerical methods must be used. The procedures for solving Equations (14) and (15) are as follows. (1) Give a value of the resonance frequency of the transducer in the all-wave vibrational mode, and from Equations (14) and (15), two values for Lc1 can be found. (2) Change the values of the resonance frequency of the transducer in the all-wave vibrational mode until the two values of L_{c1} are equal.

3. FEM Modeling

The finite element method provided by commercial ANSYS was employed for full 3D FEM modeling and analysis of the transducer to observe its vibration behavior through its simulation by modal analysis and to determine their natural frequencies by harmonic analysis. This was also for finding the validity of the analytical results. The piezoelectric transducers were modeled by using 3D method of modeling and meshing and SOLID5 elements were used for piezoelectric and other components.

Modal analysis was used to determine the natural

frequencies, mode shapes, and the location of nodal plane. This analysis was performed under resonance conditions with a constant voltage of zero being applied at all electrical contacts of ceramic disks. This is a condition of "short-circuit" where all voltage potentials are connected to common ground. No structural constraint was used for the modal analysis. This produces a simulation of an unrestrained transducer assembly. This state is similar to the state of physical testing where the transducer rests on the table with no restriction. The Block Lanczos method was chosen in this work to compute the natural frequency as this method is recommended by ANSYS instructions [16]. Mode shapes and location of nodes are shown in Figs. 6 to 9.

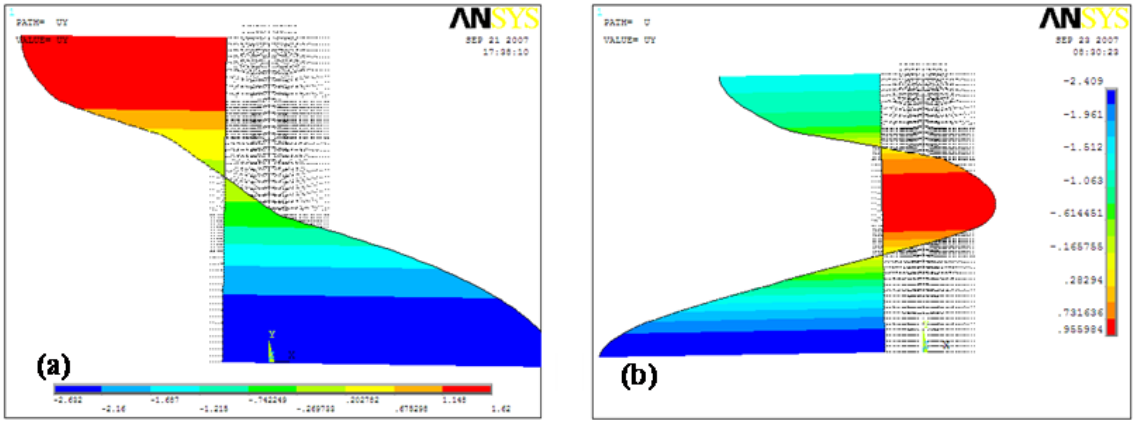

Fig. 6. The displacement distribution along longitudinal axis of SA transducer, (a) half-wave, (b) all-wave mode.

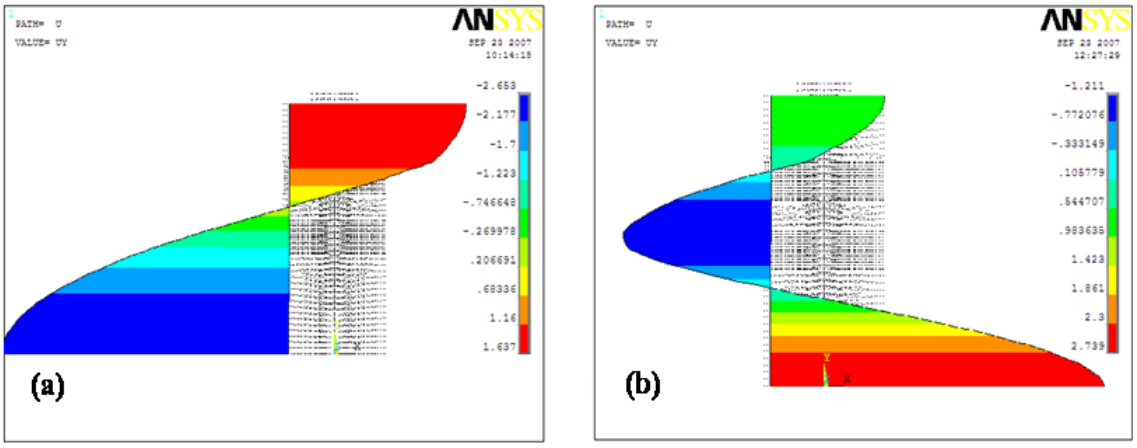

Fig. 7. The displacement distribution along longitudinal axis of AA transducer, (a) half-wave, (b) all-wave mode.

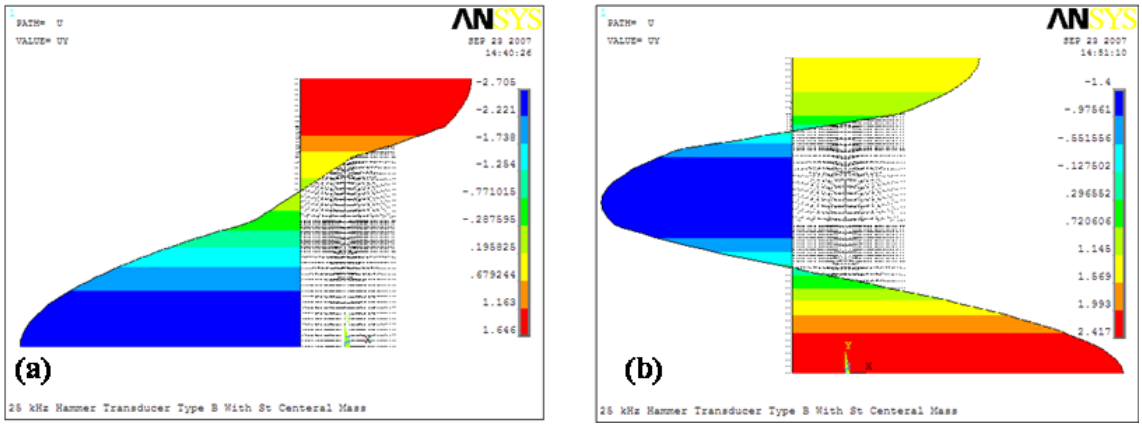

Fig. 8. The displacement distribution along longitudinal axis of SB transducer, (b) half-wave, (b) all-wave mode.

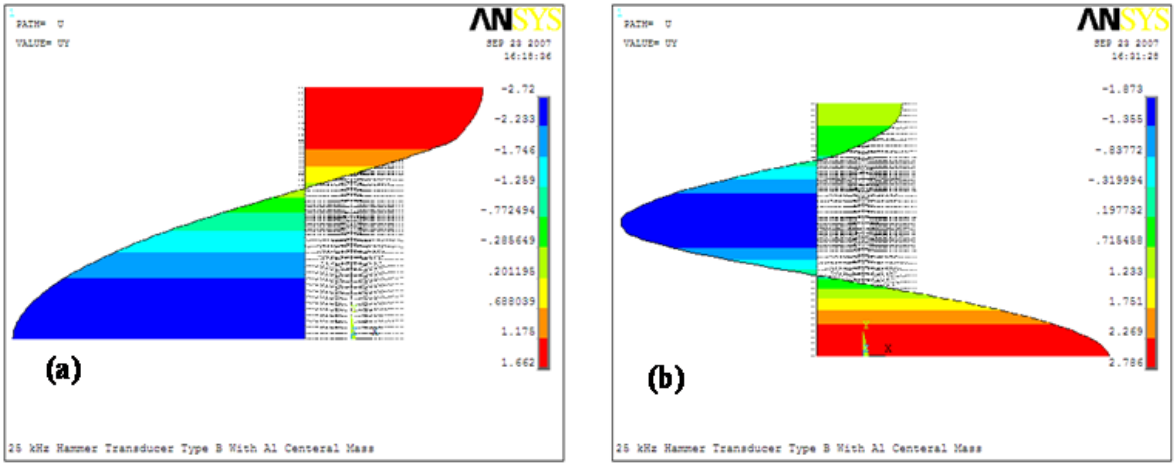

Fig. 9. The displacement distribution along longitudinal axis of AB transducer, (a) half-wave, (b) all-wave mode.

4. Experiments and Test of the Fabricated Transducers

To verify the design theory of the piezoelectric transducer with two resonance frequencies, four piezoelectric ultrasonic transducers were designed and made according to the design theory of this paper (Fig. 10). The designed and fabricated transducers were composed of four piezo-ceramic rings, PZT-SA, a steel cylinder-shaped back mass (St 304), an aluminum cylinder-shaped front mass (Al 7075-T6), a steel/aluminum cylinder-shaped central mass and a steel bolt. Table 1 shows the results obtained from analytical design of transducers with nominal frequency of 25 kHz. For the transducers design discussed in this paper, PZT-SA which is produced by TAMURA Co., was chosen as piezoelectric material. TAMURA manufacturer of piezoelectric ceramics lists the material properties of PZT-SA as [17]:
Dielectric relative permittivity matrix at constant strain, $[\varepsilon_r^2]$ (polarization axis along Y-axis):

$$[\varepsilon_r^s] = \begin{bmatrix} 874 & 0 & 0 \\ 0 & 718 & 0 \\ 0 & 0 & 874 \end{bmatrix}$$

Piezoelectric strain matrix (strain developed/electric field applied), [e] (polarization axis along Y-axis):

$$[d] = \begin{bmatrix} 0 & -131 & 0 \\ 0 & 286 & 0 \\ 0 & -131 & 0 \\ 387 & 0 & 0 \\ 0 & 0 & 387 \\ 0 & 0 & 0 \end{bmatrix} \frac{m}{V} \times 10^{-12}$$

Compliance matrix [s] under constant electric field, $[s_E]$ (polarization axis along Y-axis):

$$[s^E] = \begin{bmatrix} 11.7 & -5.17 & -3.63 & 0 & 0 & 0 \\ -5.17 & 15.5 & -5.17 & 0 & 0 & 0 \\ -3.63 & -5.17 & 11.7 & 0 & 0 & 0 \\ 0 & 0 & 0 & 33.5 & 0 & 0 \\ 0 & 0 & 0 & 0 & 33.5 & 0 \\ 0 & 0 & 0 & 0 & 30.7 & \end{bmatrix} \times 10^{-12} m^2/N$$

The most important quality quantifications of a high power ultrasonic converter (operating in certain selected resonant mode) are its quality factors equal to:

$$Q = 2\pi \frac{\text{Energy stored in the transducer during one full priode}}{\text{Energy dissipated in the transducer during one full priode}}$$

$$= 2\pi \frac{E_s}{E_d}$$

Table 1
The results obtained from analytical design of transducers with nominal frequency of 25kHz.

Central Mass	$2L_c$(mm)	L_f(mm)	L_{b1}(mm)	L_{b2}(mm)	L_p(mm)	L_{Bolt}(mm)	L_{total}(mm)
St Type A	22.5	32.1	12	6.13	10	80	93.93
Al-Type A	8.5	32.21	12	6.24	10	70	80.15
St Type B	22.5	32.582	16.367	-	10	80	92.69
Al-Type B	8.5	32.676	16.453	-	10	75	78.829

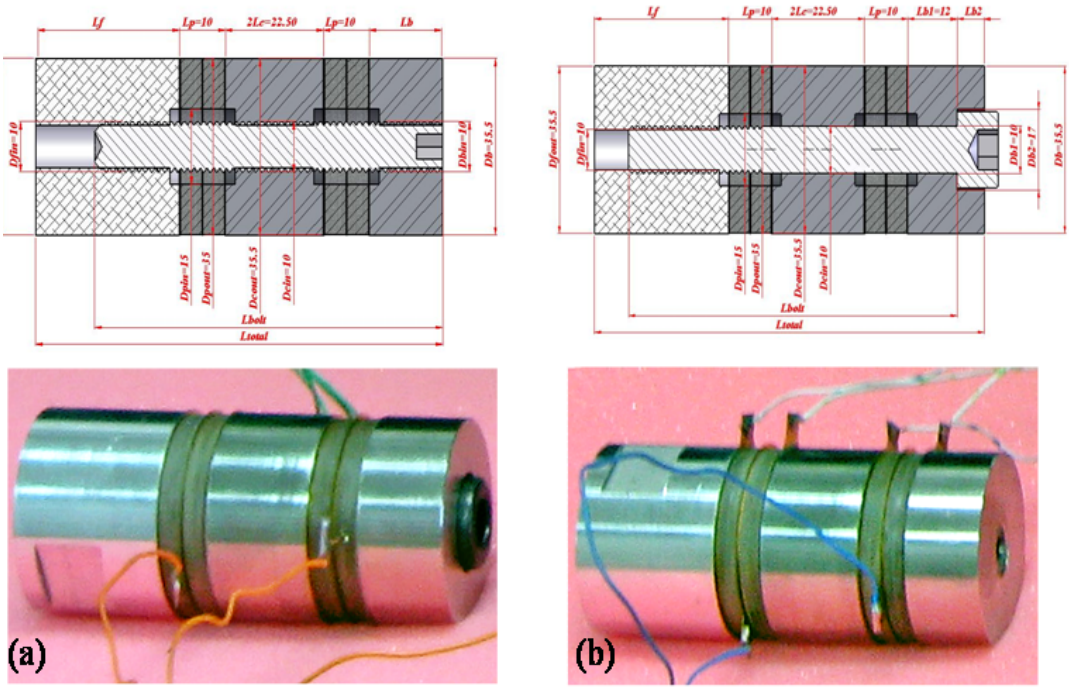

Fig. 10. The displacement distributions of AA transducer along longitudinal axis for all-wave mode.

The electric equivalent circuit of mechanically unload piezoelectric transducer is composed of series circuit R_m, L_m and C_m in parallel with C_s. The elements given in Fig. 11 are C_s; static capacitance of piezo-ceramic, L_m and C_m; equivalent motional mass and compliance elements of the transducer respectively and R_m; relates to dissipative power loss which is attributed to the joint losses.

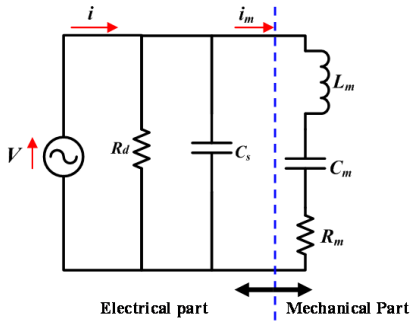

Fig. 11. The electric equivalent circuit of piezoelectric transducer.

Quality factor can be calculated (similar as in Electric Circuit Theory) for series resonance and for non-loaded piezoelectric transducer as [18]:

$$Q = \frac{Z_m}{R_m} = \frac{1}{R_m}\sqrt{\frac{L_m}{C_m}}$$

To measure the resonance frequency and determine the equivalent circuit parameters of the designed and fabricated ultrasonic transducers a precision impedance analyzer (Agilent 4294A) was employed; the sweeping frequency of this device was within 40Hz to 110MHz with a resolution of 0.001Hz. The suitable sweeping frequency was selected for each type of ultrasonic transducer and phase and impedance versus frequency diagram were drawn (Fig. 12) and the equivalent circuit parameters such as C_s, R_m, L_m, and C_m were determined. The measurement was made with the transducer unloaded. Table 2 shows the summary of the results obtained from impedance analyzer test. The index 1 and 2 refers to the first and the second mode of longitudinal vibration.

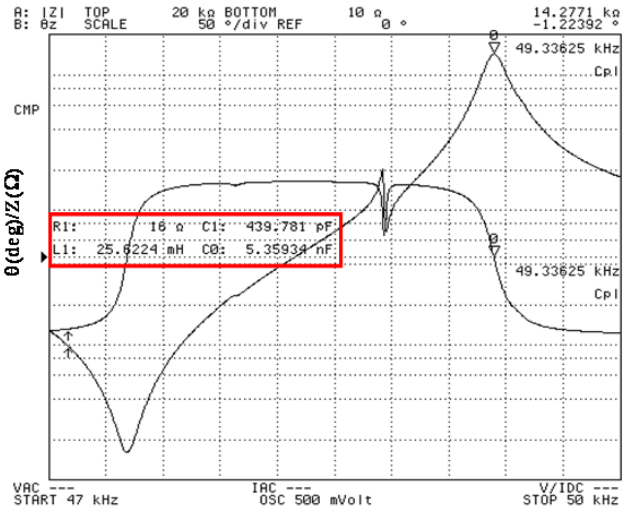

Fig. 12. The diagram of phase and impedance versus frequency generated by Impedance Analyzer for AB transducer.

Table 2
The results obtained from analytical design of transducers with nominal frequency of 25kHz.

Transducer Type	C_{01} (nf)	C_{02} (nf)	C_{m1} (nf)	C_{m2} (nf)	L_{m1} (mH)	L_{m2} (mH)	R_{m1} (Ω)	R_{m2} (Ω)
SA	6.695	5.335	0.557	0.868	51.065	18.808	94.884	22.312
AA	7.426	6.450	0.319	0.619	61.844	18.790	123.514	43.504
SB	5.532	5.663	1.488	1.398	12.433	13.125	11.921	8.140
AB	4.543	5.359	0.753	0.440	16.033	25.622	216.727Z	16.000

The determined results from analytical, FEM simulation, and experiment results are shown in Table 3, where f_{01} and f_{02} are the calculated resonance frequencies, f_{f1} and f_{f2} are the determined resonance frequencies from FEM simulation, f_{m1} and f_{m2} are the measured frequencies of the transducers in the half-wave and the all-wave vibrational modes respectively.

Table 3
The determined results from analytical, FEM simulation and experiment.

Transducer type	f_{01} (Hz)	f_{02} (Hz)	f_{f1} (Hz)	f_{f2} (Hz)	f_{m1} (Hz)	f_{m2} (Hz)	Q_1	Q_2
SA	25000	41105.5	24955	42030	230857	39390	101.03	204.62
AA	25000	50357	25196	49685	23416	46662.5	112.69	119.65
SB	25000	40355.52	25975	41746	23800	37165	242.51	412.94
AB	25000	50175.07	26138	50766	24000	47408.75	216.71	468.23

To determine the displacement distribution along longitudinal axis of transducer, the 2D Laser Doppler Vibrometer (LDV 580-2D) was used (Fig. 12). By using 2D-LDV, the speed amplitude and then displacement along longitudinal axis of transducer was determined. Figs. 13 to 16 show obtained result from experimental test and FEM modeling.

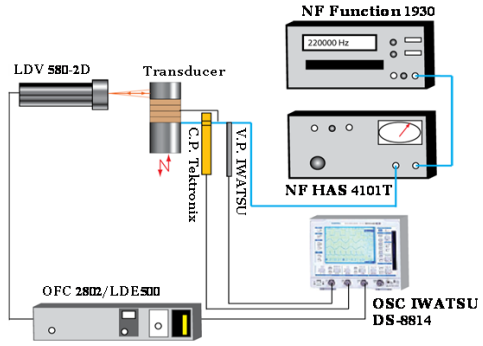

Fig. 13. Measurment setup for determination of the displacement distributions.

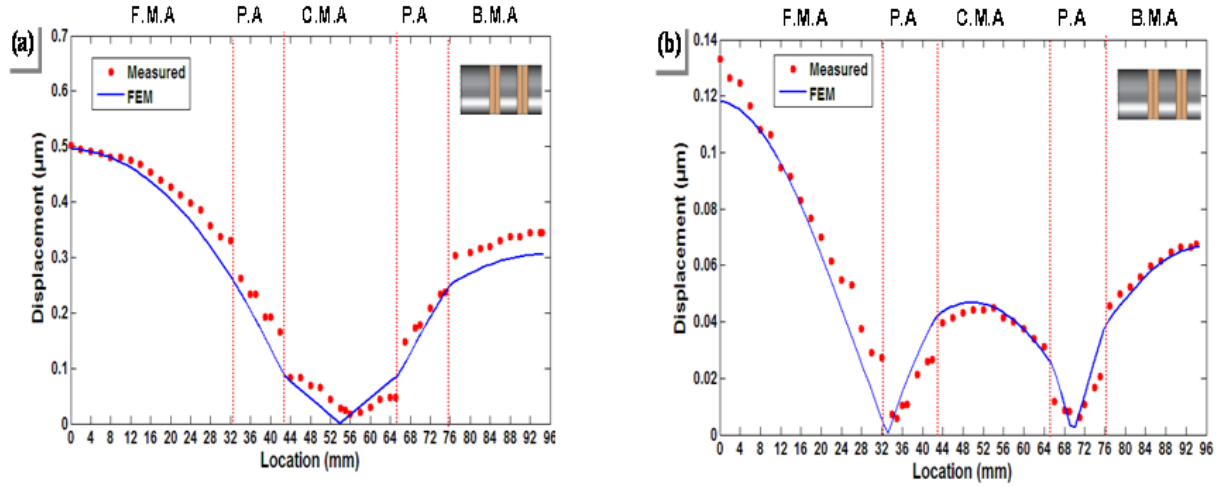

Fig. 14. The displacement distributions of SA transducer along longitudinal axis, (a) half-wave, (b) all-wave mode.

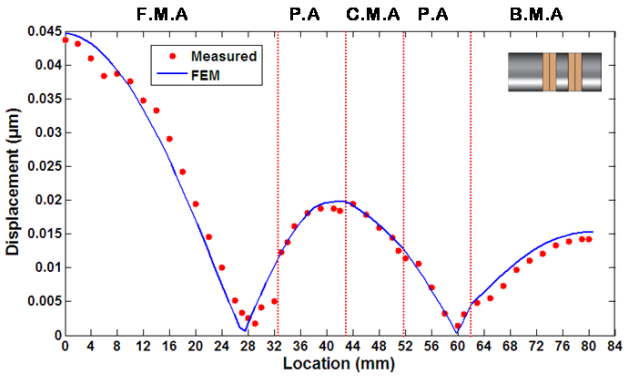

Fig. 15. The displacement distributions of AA transducer along longitudinal axis for all-wave mode.

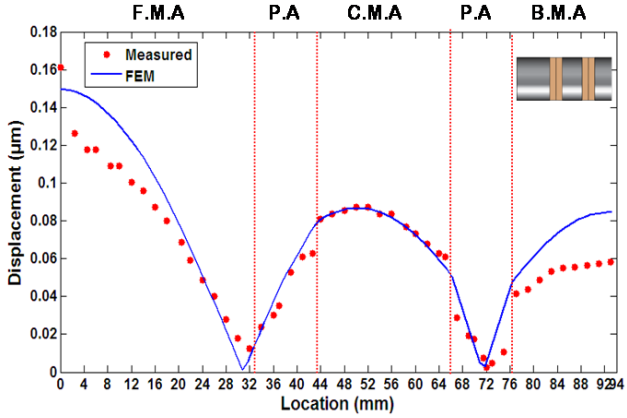

Fig. 16. The displacement distributions of SB transducer along longitudinal axis for all-wave mode.

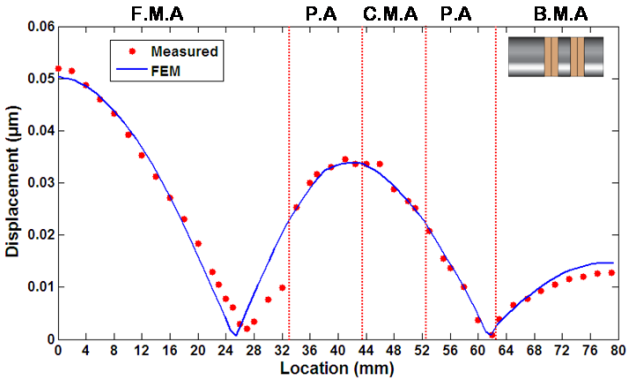

Fig. 17. The displacement distributions of AB transducer along longitudinal axis for all-wave mode.

5. Discussion

As can be seen from the Table 3, there was a difference between the measured resonance frequency and the determined resonance frequencies from FEM simulation and the intended one in designing process. This error results from the simplifications made in analyzing the wave propagation through the transducer. One of the most trouble some simplifications is assumption of one-dimensional wave propagation along the transducer which will lead to error in design of the transducer; especially to calculate the second resonance frequency of the transducers. If lateral strains are also taken into account by applying the general relationship of Youngs modulus substituted into Equation 1, the designed length of the transducer will be lower and this leads to decline of the error in frequency. In addition, interior mechanical damping of the transducer is omitted, while structural (hysteretic) damping of energy is always present in material which shifts the resonant frequency down. Furthermore, the reason of this error may be due to the ignorance of pre-stress of piezoelectric transducer. It must also be noted that this model ignores presence of the electrodes, normally used between the piezoelectric rings.

It can be seen from the data in Table 3 that Q factor for Type B transducers is better than that of Type A transducers. There are several possible explanations for this result. In Type A transducers the center mass is not directly connected to the central bolt, therefore it may move in redial direction and causes a miss elongation or matching between transducers components. Furthermore, the mechanical loss power which is attributed to the joint losses from planar friction losses between piezoelectric rings and other components (baking and center mass) in Type A transducer are more than those of Type B transducers. As Table 2 shows, R_m that relates to dissipative power loss for Type A transducers more than Type B transducers.

As shown in Figs. 13 to 16, there is a good agreement between the experimental and FEM results for the displacement distribution along longitudinal axis of transducer for all transducers.

6. Conclusions

In this study, two configurations of the piezoelectric ultrasonic transducer with two resonance frequencies were analyzed by theoretical, numerical, and experimental methods and four transducers were developed and tested. The study presented in this paper concludes:

1. It was found that the analyzed transducers have two resonance frequencies that correspond to the half-wave and the all-wave vibrational modes.

2. Comparison of the results obtained from FEM simulation proved that there is a good agreement between the results achieved from the analytical and the FEM modeling.

3. It can be seen from the Table 2 compared with measured frequency, there is a small difference between resonance frequencies obtained from the analytical and the FEM modeling. The reason

of this error may be due to simplifying presumption of one-dimensional wave propagation along the transducer and the ignorance of pre-stress of piezoelectric transducer and the mechanical loss power attributed to the joint losses from planar friction losses between piezoelectric and metal parts and to the material hysteretic-related losses (internal mechanical damping in all transducer parts).

4. There is a good agreement between the experimental and FEM results for the displacement distribution along longitudinal axis of transducer.

5. As shown in the Table 2 that use of type B transducer increased the mechanical quality factor (Q) of dual piezoelectric transducers.

6. There is a possibility of achieving the various second resonance frequencies with same first resonance frequency by using different center mass material.

7. The results obtained are showing that the capabilities of the ANSYS software can be used successfully as a powerful and reliable tool for prediction of behavior of multifrequency piezoelectric transducers.

Acknowledgements

The authors express their sincere appreciation to Prof. Ueha and Prof. Nakamura for their contribution in conducting some of the experiments for the research. Thanks should also be given to Precision and Intelligence Laboratory at Tokyo Institute of Technology for providing experimental facilities.

References

[1] L. Shuyu, Study on the multifrequency Langevin ultrasonic transducer, Ultrasonics, 33(6) (1995) 445-448.

[2] Y.R. Yeon-bo Kim, New design of matching layers for high power and wide band ultrasonic transducers, Sensor. Actuator., 71 (1998) 116-122.

[3] L. Parrini, Design of advanced ultrasonic transducers for welding devices, IEEE Trans. Ultrason., Ferroelect., Freq. Control., 48(6) (2001) 1632-1639.

[4] B. Dubus, G. Haw, C. Granger, O. Ledez, Characterization of multilayered piezoelectric ceramics for high power transducers, Ultrasonics, 40 (2002) 903-906.

[5] H.L.W. Chan, M.W. Ng, P.C.K. Liu, Effect of hybrid structure (1/3 composite and ceramic) on the performance of sandwich transducers, Mat. Sci. Eng., B99 (2003) 6-10.

[6] S. Saitoh, M. Izumi, Y. Mine, A dual frequency ultrasonic probe for medical applications, IEEE Trans. Ultrason. Ferroelectr. Freq. Control, 42 (1995) 294-300.

[7] G. Piazza, P.J. Stephanou, A. Pisano, Single-chip multiple-frequency AlN MEMS filters based on contour-mode piezoelectric resonators, J. Microelectromech. Syst., 16 (2007) 319-28, .

[8] K. Heath Martin, B.D. Lindsey, J. Ma, M. Lee, S. Li, F.S. Foster , X. Jiang, P.A. Dayton, Dual-frequency piezoelectric transducers for contrast enhanced ultrasound imaging, Sensors, 14 (2014) 20825-20842.

[9] S. Lin, C. Xu, Analysis of the sandwich ultrasonic transducer with two sets of piezoelectric elements, Smart. Mater. Struct., 17(6) (2008) **6** 065008.

[10] S. Lin, An improved cymbal transducer with combined piezoelectric ceramic ring and metal ring, Sensor. Actuator., 163(1) (2010) 266-276.

[11] S. Lin, L. Xu, H. Wenxu, A new type of high power composite ultrasonic transducer, J. Sound. Vib., 330(7) (2011) 1419-1431.

[12] Ş. Deniz, The design of a multi-frequency underwater acoustic transducer with cylindrical piezoelectric elements, MSc Thesis. Turkey: Middle East Technical University; 2011.

[13] T. Asami, H. Miura, Longitudinaltorsional vibration source consisting of two transducers with different vibration modes, JPN. J. Appl. Phys., 55 (2016) 7-8.

[14] J.W. Rayleigh, The Theory of Sound, New York, 1945.

[15] K.F. Graff, Wave Motion in Elastic Solids, Oxford University Press, 1975.

[16] R.G. Grimes, J.G. Lewis, H.D. Simon, A shifted block lanczos algorithm for solving sparse systematic generalized eigenproblems, Siam. J. Matrix. Anal. Appl., 15 (1994) 228-272.

[17] Piezoelectric Ceramics for High Power Applications data sheet, TAMURA CO., 2006.

[18] G.W. Taylor., J.J. Gagnepain, Piezoelectricity, New York: Gordon and Breach Science, 4 (1960).